Theory of elastic interaction between arbitrary colloidal particles in confined nematic liquid crystals

O. M. Tovkach,[1] S. B. Chernyshuk,[2] and B. I. Lev[1]
[1]*Bogolyubov Institute for Theoretical Physics, NAS Ukraine, Metrologichna 14-b, Kyiv 03680, Ukraine*
[2]*Institute of Physics, NAS Ukraine, Prospekt Nauki 46, Kyiv 03650, Ukraine*
(Received 15 August 2012; revised manuscript received 23 November 2012; published 26 December 2012)

We develop the method proposed by Chernyshuk and Lev [Phys. Rev. E **81**, 041701 (2010)] for theoretical investigation of elastic interactions between colloidal particles of arbitrary shape and chirality (polar as well as azimuthal anchoring) in the confined nematic liquid crystal (NLC). General expressions for six different types of multipole elastic interactions are obtained in the confined NLC: monopole-monopole (Coulomb type), monopole-dipole, monopole-quadrupole, dipole-dipole, dipole-quadrupole, and quadrupole-quadrupole interactions. The obtained formulas remain valid in the presence of the external electric or magnetic fields. The exact equations are found for all multipole coefficients for the weak anchoring case. For the strong anchoring coupling, the connection between the symmetry of the shape or director and multipole coefficients is obtained, which enables us to predict which multipole coefficients vanish and which remain nonzero. The particles with azimuthal helicoid anchoring are considered as an example. Dipole-dipole interactions between helicoid cylinders and cones are found in the confined NLC. In addition, the banana-shaped particles in homeotropic and planar nematic cells are considered. It is found that the dipole-dipole interaction between banana-shaped particles differs greatly from the dipole-dipole interaction between the axially symmetrical particles in the nematic cell. There is a crossover from attraction to repulsion between banana particles along some directions in nematic cells. It is shown that monopoles do not "feel" the type of nematic cell: monopole-monopole interaction turns out to be the same in homeotropic and planar nematic cells and converges to the Coulomb law as thickness increases, $L \to \infty$.

DOI: 10.1103/PhysRevE.86.061703 PACS number(s): 61.30.−v, 42.70.Df, 64.70.pv, 47.57.J−

I. INTRODUCTION

The world of nematic liquid crystal (NLC) colloids is much more diverse than the world of the usual isotropic colloids. Particles suspended in a nematic liquid crystal host distort the orientational nematic order on distances much larger than their size. Distortions intersect and interact with each other, giving rise to the effective elastic interactions between colloidal particles. These anisotropic elastic interactions resemble electrostatic interactions, but sometimes they are very different. They never occur in isotropic hosts, and they result in the formation of different colloidal structures in liquid crystals. For instance, spherical water droplets in the NLC may produce a hedgehog director configuration which has asymptopic dipole director symmetry. The dipole director symmetry causes effective dipole-dipole-type elastic interaction between droplets and produces linear chains along the average director field $\mathbf{n}_0$ [1–4]. At the same time, glycerol spherical droplets with planar anchoring at the surface produce director deviations with quadrupole symmetry which cause aggregations of droplets into the incline chains [3,5–7].

The authors of [5] found that solid microspheres with planar anchoring form chains directed at 30° to $\mathbf{n}_0$. Colloids suspended at the nematic-air interface produce director deformations in the bulk and distort the surface of the LC. This elastic-capillary coupling leads to the formation of two-dimensional (2D) hexagonal structures with different lattice constants [8,9]. Photochemical switching between those structures induced by laser light was directly observed in Refs. [10,11]. Transformation of the 2D colloidal hexagonal lattice at the nematic interface into the chains under the action of the magnetic field was found in Ref. [12].

One can obtain a rich variety of 2D crystals by laser tweezer manipulations with colloids in thin nematic cells. In particular, there are 2D hexagonal quadrupole crystals [13], antiferroelectric-like 2D crystals of dipolar particles [13,14], and mixed 2D crystals [15] sandwiched between cell walls. The authors of [16] reported that similar superstructures were possible in mixtures of small and large colloidal particles as well. In such systems, small particles are arranged in a matrix of topological defects produced by large colloids. Another interesting issue is 1D structures bound by delocalized topological defects. These so called colloidal wires could have some applications as, for example, optical waveguides. The possibility of their existence was confirmed in Ref. [17]. Two-dimensional colloidal crystals assembled from chiral colloidal dimers in a twisted nematic cell were found in Ref. [18]. Many experimental results were reproduced with the Landau–de Gennes free-energy numerical minimization [13–27] as well as by molecular-dynamics simulations [28].

A theoretical understanding of the matter in the bulk NLC has deep analogy with classical electrostatics. Indeed, far from the particle, the director field deviations are guided by the Laplace equation and can be expanded in multipoles. This fact became a starting point for a number of approaches toward the theory of NLC colloids [29–34]. But only one of them, [29], gives exact analytical quantitative results which have been proven experimentally in the bulk nematic LC. The authors of [4] measured directly the dipole-dipole interaction between two spherical iron particles in a magnetic field and found it to be in accordance with [29] within a few percent accuracy. This allows us to justify the main assumptions of [29] for spherical particles in the bulk nematic liquid crystal. Recently, the authors of [25,26] developed a numerical method which allows us to calculate the interparticle force between two particles of different sizes. They found numerical results in good agreement with their own experimental

data as well as with the predictions of the electrostatic analogy.

But in practice, liquid crystals are always confined with some surfaces and their influence cannot be neglected. The authors of [19,20] have found experimentally that the interactions in the nematic cell are exponentially screened across distances comparable to the cell thickness L (the so called confinement effect). Qualitative theoretical investigations of the surface effects on the elastic interaction between beads in the confined NLC were performed in Refs. [35–39]. References [35–37] are based on the "coat" concept (introduced in Ref. [31]) which enables us to find the correct analytical form of the potentials up to the unknown multiplicative constant.

Not so long ago, a proposal was made [40–42] to extend the method [29] on the confined NLC and to find the exact analytical form of all elastic potentials. Using that approach, the elastic interactions between axially symmetric particles were found in the nematic cell and near one wall with either planar or homeotropic boundary conditions. The proposed theory [40,41] fits very well with the experimental data for the confinement effect between spheres in the homeotropic cell [19] in the range 1–1000 kT as well as the confinement effect in the planar cell for different cell thicknesses L [20].

But all those results were obtained for the beads or axially symmetric particles. In this paper, we generalize the approach [29,40–42] for the particles *of arbitrary shape and chirality*. We obtain general formulas for the elastic interaction potential between such colloidal particles in the confined NLC. The only particles' characteristics which determine elastic interactions are the multipole coefficients which describe the director field deformations far from the particle. We make the analysis of the multipole coefficients from a symmetry point of view and classify them in dependence on the shape symmetry. This provides a way to determine which coefficients vanish and which remain nonzero depending on the director symmetry around the particles. The proposed analysis is valid for the cases of weak as well as *strong* anchoring coupling constant W. We consider both cases of the *polar and azimuthal* anchoring coupling at the particle surface, and we analyze the possible chirality of colloidal particles. Thus the proposed approach covers the main possible shapes and director configurations around colloidal particles in the confined NLC as well as interactions between them.

In Sec. II, we generalize the method [40,41] and obtain the most general expressions for the elastic interactions between colloidal particles. In Sec. III, we connect multipole coefficients with the symmetry of the director field around the particle.

In Sec. IV, we consider the dipole-dipole interaction between two identical banana-shaped particles in a nematic cell. Finally, the monopole-monopole interaction in homeotropic and planar nematic cells is briefly discussed in Sec. V.

II. ELASTIC INTERACTIONS IN NEMATIC LIQUID CRYSTAL COLLOIDS

Let us consider a liquid crystal colloidal system consisting of a nematic host and one suspended particle. Anchoring of the liquid crystal with the particle's surface produces deformations of the director field $\mathbf{n}$, so that $\mathbf{n}$ varies from point to point. The total energy of the system is presented as a sum of the bulk and surface free energies $F = F_{\text{bulk}} + F_{\text{surface}}$. The bulk energy of these deformations can be written as

$$F_{\text{bulk}} = \frac{K}{2}\int dV[(\nabla\cdot\mathbf{n})^2 + (\nabla\times\mathbf{n})^2], \tag{1}$$

where K is the Frank elastic constant. We use the one-constant approximation, $K_{11} = K_{22} = K_{33} = K$, and omit the K_{24} term because it does not play a crucial role in further considerations [41]. Surface energy $F_{\text{surface}} \propto W$ is proportional to the anchoring strength coefficient W and will be discussed in more detail in Sec. III [see (20)].

Far from the particle director, the field variations are small, $\mathbf{n}(\mathbf{r}) \approx (n_x, n_y, 1)$, $|n_\mu| \ll 1$. Hereafter, $\mu = \{x, y\}$ and $\mathbf{n}_0 = (0,0,1)$ is the ground state of pure nematic liquid crystal. Thus the bulk free energy reduces to the harmonic free energy

$$F_{\text{bulk}} = \frac{K}{2}\int dV(\nabla n_\mu)^2, \tag{2}$$

and repeated μ means summation on x and y like $(\nabla n_\mu)^2 = (\nabla n_x)^2 + (\nabla n_y)^2$. The Euler-Lagrange equations for n_μ are of the Laplace type,

$$\Delta n_\mu = 0. \tag{3}$$

Similarly as in classical electrostatics, the solutions of these equations can be expanded in multipoles,

$$n_\mu(\mathbf{r}) = \frac{q_\mu}{r} + \frac{p_\mu^\alpha r_\alpha}{r^3} + \frac{Q_\mu^{\alpha\beta} r_\alpha r_\beta}{r^5} + \cdots, \tag{4}$$

where α and β take values x, y, z, and summation over repeated greek indices is assumed. Quantities q_μ, p_μ^α, and $Q_\mu^{\alpha\beta}$ are called elastic charges (monopoles), dipoles, and quadrupoles, respectively. At large distances r, the multipole expansion is valid regardless of the anchoring strength. Hence, the long-range interactions in NLC colloids are always controlled by multipole coefficients. In a general case, these multipole coefficients can be found as fitting parameters for agreement with experimental data.

As follows from (4), director deviations n_x and n_y have a long-range nature. This means that deformations caused by different particles can overlap even if the particles are located far from each other. In practice, the overlapping manifests itself in the fact that a colloidal particle "feels" the presence of the other particles mediated by a nematic host, and this leads to the appearance of the effective long-range interactions between colloidal particles. Since far from the particle the multipole expansion (4) is valid regardless of the anchoring strength, all these interactions are determined precisely by the coefficients q_μ, p_μ^α, $Q_\mu^{\alpha\beta}$.

Now let us imagine that we have found all these multipole coefficients in some way, so that we know two elastic charges q_μ, six components of the dipole moment p_μ^α, and five components of the quadrupole moment $Q_\mu^{\alpha\beta}$ for every $\mu = \{x, y\}$ (10 altogether). Note that the quadrupole moment tensor $\hat{Q}_\mu = \{Q_\mu^{\alpha\beta}\}$ can always be introduced in such a way that it would be a symmetric, $Q_\mu^{\alpha\beta} = Q_\mu^{\beta\alpha}$, and traceless one, $\mathrm{Sp}\hat{Q}_\mu = Q_\mu^{\alpha\beta}\delta_{\alpha\beta} = 0$ [44]. So we have 18 multipole parameters. Now we need to build some effective free-energy functional, which includes the multipole coefficients and gives

the correct behavior of the director at large distances from the particle.

This aim was achieved in Ref. [29] for the case of axially symmetric particles. The effective free-energy functional was written as

$$F_{\rm eff}^{\rm axial\text{-}sym} = K\int dV\Big[\frac{(\nabla n_\mu)^2}{2} - 4\pi P(\mathbf{x})\partial_\mu n_\mu - 4\pi C(\mathbf{x})\partial_z\partial_\mu n_\mu\Big], \quad (5)$$

where $P(\mathbf{x}) = p\delta(\mathbf{x})$ and $C(\mathbf{x}) = Q\delta(\mathbf{x})$ are dipole and quadrupole moment densities and $\partial_\mu n_\mu = \partial_x n_x + \partial_y n_y$.

Obviously the generalization of this effective free-energy functional for particles of arbitrary shape and anchoring strength can be presented in the form

$$F_{\rm eff} = K\int dV\Big[\frac{(\nabla n_\mu)^2}{2} - 4\pi q_\mu(\mathbf{x})n_\mu - 4\pi p_\mu^\alpha(\mathbf{x})\partial_\alpha n_\mu - 4\pi Q_\mu^{\alpha\beta}(\mathbf{x})\partial_\alpha\partial_\beta n_\mu\Big], \quad (6)$$

where $q_\mu(\mathbf{x}) = q_\mu\delta(\mathbf{x})$, $p_\mu^\alpha(\mathbf{x}) = p_\mu^\alpha\delta(\mathbf{x})$, and $Q_\mu^{\alpha\beta}(\mathbf{x}) = Q_\mu^{\alpha\beta}\delta(\mathbf{x})$ are pointlike densities; α and β take values x,y,z, and summation over repeated greek indices $\mu = x,y$ is assumed. In the case of axially symmetric particles without helical twisting, $q_\mu = 0, p_\mu^\alpha = 0$ except $p_x^x = p_y^y = p$ and $Q_x^{xz} = Q_x^{zx} = Q_y^{yz} = Q_y^{zy} = Q$ and we come to (5).

The Euler-Lagrange equations arising from (6) are Poisson equations,

$$\Delta n_\mu = -4\pi q_\mu(\mathbf{x}) + 4\pi\big[\partial_\alpha p_\mu^\alpha(\mathbf{x}) - \partial_\alpha\partial_\beta Q_\mu^{\alpha\beta}(\mathbf{x})\big]. \quad (7)$$

If the liquid crystal is confined by some surface Σ so that $n_\mu|_\Sigma = 0$, then solutions of (7) are

$$n_\mu = \int_V dV' G_\mu(\mathbf{x},\mathbf{x}')\big[q_\mu(\mathbf{x}') - \partial'_\alpha p_\mu^\alpha(\mathbf{x}') - \partial'_\alpha\partial'_\beta Q_\mu^{\alpha\beta}(\mathbf{x}')\big], \quad (8)$$

where $G_\mu(\mathbf{x},\mathbf{x}')$ are Green's functions, $\Delta G_\mu(\mathbf{x},\mathbf{x}') = -4\pi\delta(\mathbf{x}-\mathbf{x}')$ for any $\mathbf{x},\mathbf{x}' \in V$, and $G_\mu(\mathbf{x},\mathbf{s}) = 0$ for any $\mathbf{s} \in \Sigma$. When the nematic is unlimited, $G_\mu(\mathbf{x},\mathbf{x}') = \frac{1}{|\mathbf{X}-\mathbf{X}'|}$ and (8) yields (4).

Due to the linearity of the Euler-Lagrange equations (7), we can use the superposition principle for the system of N colloidal particles,

$$q_\mu(\mathbf{x}) = \sum_{i=1}^N q_{\mu,i}\delta(\mathbf{x}-\mathbf{x}_i),$$
$$p_\mu^\alpha(\mathbf{x}) = \sum_{i=1}^N p_{\mu,i}^\alpha\delta(\mathbf{x}-\mathbf{x}_i), \quad (9)$$
$$Q_\mu^{\alpha\beta}(\mathbf{x}) = \sum_{i=1}^N Q_{\mu,i}^{\alpha\beta}\delta(\mathbf{x}-\mathbf{x}_i),$$

so that the director field distortions are the sum of distortions caused by every single particle. Substituting (8) into (6) and implying (9), we come to the fact that the free energy of the system can be presented as a sum of the self-energy part and pair interactions $F_{\rm eff} = U^{\rm self} + U^{\rm interaction}$, where $U^{\rm self} = \sum_i U_i^{\rm self}$ and

$$U^{\rm interaction} = \sum_i\sum_{j<i} U^{ij}(\mathbf{x}_i,\mathbf{x}_j). \quad (10)$$

The pair elastic interaction U^{ij}, in turn, is the sum of monopole-monopole, monopole-dipole, monopole-quadrupole, dipole-dipole, dipole-quadrupole, and quadrupole-quadrupole interactions, $U^{ij} = U_{\rm qq} + U_{\rm qd} + U_{\rm qQ} + U_{\rm dd} + U_{\rm dQ} + U_{\rm QQ}$, where

$$U_{\rm qq} = -4\pi K\, q_{\mu,i}\, q_{\mu,j}\, G_\mu(\mathbf{x}_i,\mathbf{x}'_j), \quad (11)$$

$$U_{\rm qd} = -4\pi K\big\{q_{\mu,i}\, p_{\mu,j}^\alpha\, \partial'_\alpha G_\mu(\mathbf{x}_i,\mathbf{x}'_j) + q_{\mu,j}\, p_{\mu,i}^\alpha\, \partial_\alpha G_\mu(\mathbf{x}_i,\mathbf{x}'_j)\big\}, \quad (12)$$

$$U_{\rm qQ} = -4\pi K\big\{q_{\mu,i}\, Q_{\mu,j}^{\alpha\beta}\, \partial'_\alpha\partial'_\beta G_\mu(\mathbf{x}_i,\mathbf{x}'_j) + q_{\mu,j}\, Q_{\mu,i}^{\alpha\beta}\, \partial_\alpha\partial_\beta G_\mu(\mathbf{x}_i,\mathbf{x}'_j)\big\}, \quad (13)$$

$$U_{\rm dd} = -4\pi K\, p_{\mu,i}^\alpha\, p_{\mu,j}^\beta\, \partial_\alpha\partial'_\beta G_\mu(\mathbf{x}_i,\mathbf{x}'_j), \quad (14)$$

$$U_{\rm dQ} = -4\pi K\big\{p_{\mu,i}^\alpha\, Q_{\mu,j}^{\beta\gamma}\, \partial_\alpha\partial'_\beta\partial'_\gamma G_\mu(\mathbf{x}_i,\mathbf{x}'_j) + p_{\mu,j}^\alpha\, Q_{\mu,i}^{\beta\gamma}\, \partial'_\alpha\partial_\beta\partial_\gamma G_\mu(\mathbf{x}_i,\mathbf{x}'_j)\big\}, \quad (15)$$

$$U_{\rm QQ} = -4\pi K\, Q_{\mu,i}^{\alpha\beta}\, Q_{\mu,j}^{\gamma\delta}\, \partial_\alpha\partial_\beta\partial'_\gamma\partial'_\delta G_\mu(\mathbf{x}_i,\mathbf{x}'_j). \quad (16)$$

Expressions (11)–(16) are general formulas for the long-range elastic pair interaction potentials between colloidal particles of arbitrary shape in the confined NLC. In the bulk NLC, we should take $G_\mu(\mathbf{x},\mathbf{x}') = \frac{1}{|\mathbf{X}-\mathbf{X}'|}$.

The self-energy part (the energy of the one particle in the confined NLC or the energy of the interaction with confining walls) can also be presented as the sum $U_i^{\rm self} = U_{\rm qq}^{\rm self} + U_{\rm qd}^{\rm self} + U_{\rm qQ}^{\rm self} + U_{\rm dd}^{\rm self} + U_{\rm dQ}^{\rm self} + U_{\rm QQ}^{\rm self}$, where all $U_{\rm AB}^{\rm self}$ are obtained using the formulas (11)–(16) but $G_\mu(\mathbf{x}_i,\mathbf{x}'_j)$ should be replaced with $H_\mu(\mathbf{x}_i,\mathbf{x}'_j)$ [where $G_\mu(\mathbf{x},\mathbf{x}') = \frac{1}{|\mathbf{X}-\mathbf{X}'|} + H_\mu(\mathbf{x},\mathbf{x}')$ and $\Delta_{\mathbf{X}} H_\mu(\mathbf{x},\mathbf{x}') = 0$] and it is necessary to set $\mathbf{x}'_j = \mathbf{x}_i$ after all primed derivatives ∂'_ξ are taken out. In this way, we exclude the divergent part of the self-energy coming out from $\frac{1}{|\mathbf{X}-\mathbf{X}'|}$ and retain only the regular part $U_i^{\rm self}$ coming from $H_\mu(\mathbf{x},\mathbf{x}')$. Using this procedure, we can find that

$$U_{\rm qq}^{\rm self} = -4\pi K q_{\mu,i}\, q_{\mu,i}\, H_\mu(\mathbf{x}_i,\mathbf{x}_i), \quad (17)$$

$$U_{\rm qd}^{\rm self} = -4\pi K\big[q_{\mu,i}\, p_{\mu,i}^\alpha\, \partial'_\alpha H_\mu(\mathbf{x}_i,\mathbf{x}'_i) + q_{\mu,i}\, p_{\mu,i}^\alpha\, \partial_\alpha H_\mu(\mathbf{x}_i,\mathbf{x}'_i)\big]\big|_{\mathbf{x}_i=\mathbf{x}'_i}, \quad (18)$$

$$U_{\rm dd}^{\rm self} = -4\pi K\, p_{\mu,i}^\alpha\, p_{\mu,i}^\beta\, \partial_\alpha\partial'_\beta H_\mu(\mathbf{x}_i,\mathbf{x}'_i)|_{\mathbf{x}_i=\mathbf{x}'_i}, \ldots, \quad (19)$$

etc.

All these formulas (11)–(19) remain valid even when external electric $\mathbf{E}$ or magnetic $\mathbf{H}$ fields are applied to the confined NLC (that was proved in Ref. [42] for axially symmetric particles), but Green's functions $G_\mu(\mathbf{x}_i,\mathbf{x}'_j)$ should be substituted with $G_\mu^{\rm field}(\mathbf{x}_i,\mathbf{x}'_j)$. Rigorous proof of this statement is the same as in Ref. [42], so we omit it here. Those Green's functions $G_\mu^{\rm field}(\mathbf{x}_i,\mathbf{x}'_j)$ were found in Ref. [42] for the homeotropic and planar nematic cells and for different

orientations of the field **E**. Direct use of them in Eqs. (11)–(16) gives interaction between arbitrary colloidal particles in the confined NLC in the presence of the fields **E** or **H**.

Formulas (11)–(16) show that the energy of interaction depends on both multipole coefficients and Green's functions. The former originate from the interaction between the particle surface and NLC molecules. The latter are determined by the shape of the confining surface Σ as well as by external fields **E** or **H**.

III. MULTIPOLE COEFFICIENTS AND PARTICLE SYMMETRY

In this section, we want to establish a connection between the symmetry of the particle and the director deformations produced at large distances. As mentioned above, these distortions are completely described by a set of multipole coefficients $q_\mu, p_\mu^\alpha, Q_\mu^{\alpha\beta}$. Strictly speaking, we should distinguish two cases here. When the anchoring is weak, $\mathrm{Wr}_0/K < 1$ (r_0 being the average size of the particle), the deformations are small everywhere outside the particle and the coefficients can be found from the mechanical equilibrium condition (we apply this procedure below). If the anchoring is strong, $\mathrm{Wr}_0/K > 1$, the deformations in the particle's vicinity are large, and even topological defects may appear there. So the coefficients cannot be linked directly to the particle's symmetry. But in this case the notion of the coat suggested in Ref. [31] is helpful. The coat is an area that contains all topological defects and large deformations inside, so that the director field outside is presented in the form of multipole expansion (4). The symmetry of the coat matches with the symmetry of the director field around the particle and can be easily observed experimentally. In fact, one can treat the coat as some imaginary particle with appropriate symmetry and weak anchoring on its surface. Therefore, from this point on we only use the term "particle."

Thus, it is enough to consider one colloidal particle with weak anchoring in a bulk NLC. The free energy of such a system is the sum of two parts: bulk energy (2) and the surface anchoring energy. The latter can be presented as

$$F_{\mathrm{surface}} = \oint dS\, W^{\alpha\beta}(\mathbf{s}) n_\alpha(\mathbf{s}) n_\beta(\mathbf{s}), \tag{20}$$

where $W^{\alpha\beta}(\mathbf{s})$ is the symmetrical local anchoring tensor at point **s** on the particle's surface [43]. The tensor description has a covariant form and describes both polar and azimuthal anchoring simultaneously. But a connection between the particle's symmetry and the tensor's properties is not so clear in the general case. To make our analysis as transparent as possible, we should use the following representation of the surface energy:

$$F_{\mathrm{surface}} = \oint dS\, W_p(\mathbf{s})[\boldsymbol{\nu}(\mathbf{s})\cdot\mathbf{n}(\mathbf{s})]^2 - \oint dS\, W_a(\mathbf{s})[\boldsymbol{\tau}(\mathbf{s})\cdot\mathbf{n}(\mathbf{s})]^2. \tag{21}$$

This is the generalized Rapini-Popular surface energy, with W_p and W_a being the strengths of the polar and azimuthal anchoring energies, respectively. Here $\boldsymbol{\nu}$ is the outer normal to the particle's surface at the point **s**, and $\boldsymbol{\tau}$ is the unit tangential vector along the local rubbing, which also depends on the point **s** of the surface. Azimuthal anchoring $W^a > 0$ results in alignment of the director along vector field $\boldsymbol{\tau}(\mathbf{s})$ at the surface. Since the anchoring is weak, the total energy can be reduced to

$$F_{\mathrm{harm}} = \frac{K}{2}\int dV(\nabla n_\mu)^2 + 2\oint dS\, W_p(\mathbf{s})\nu_z(\mathbf{s})\nu_\mu(\mathbf{s})n_\mu(\mathbf{s}) - 2\oint dS\, W_a(\mathbf{s})\tau_z(\mathbf{s})\tau_\mu(\mathbf{s})n_\mu(\mathbf{s}), \tag{22}$$

where we neglected terms like $(\nabla n_z)^2$, $W_p n_\mu n_{\mu'}$, and $W_a n_\mu n_{\mu'}$ because of their smallness. Note that, in fact, $W_p\nu_z\nu_\mu - W_a\tau_z\tau_\mu = W^{z\mu}$ in Eq. (20).

At the same time, the director field everywhere outside the particle in the unlimited NLC is described by (4), so that

$$(\nabla n_\mu)^2 = \frac{q_\mu q_\mu}{r^4} + \sum_{\alpha,\beta,\gamma,\delta}\frac{p_\mu^\alpha p_\mu^\alpha}{r^6} + 3\frac{p_\mu^\alpha r_\alpha p_\mu^\beta r_\beta}{r^8} + 5\frac{Q_\mu^{\alpha\beta}r_\alpha r_\beta Q_\mu^{\gamma\delta}r_\gamma r_\delta}{r^{12}} + 4\frac{Q_\mu^{\alpha\gamma}Q_\mu^{\beta\gamma}r_\alpha r_\beta}{r^{10}} + 4\frac{q_\mu p_\mu^\alpha r_\alpha}{r^6} + 6\frac{q_\mu Q_\mu^{\alpha\beta}r_\alpha r_\beta}{r^8} + 8\frac{p_\mu^\alpha Q_\mu^{\beta\gamma}r_\alpha r_\beta r_\gamma}{r^{10}} + 4\frac{p_\mu^\alpha Q_\mu^{\alpha\beta}r_\beta}{r^8}. \tag{23}$$

Then substituting (4) and (23) into (22) and performing the integration, one can obtain the free energy of the system as a function of the multipole coefficients,

$$F_{\mathrm{harm}} = \frac{1}{2}\sum_{uv} a_{uv}m_u m_v + \sum_u c_u m_u, \tag{24}$$

where we introduced the vector of the coefficients $\mathbf{m} = (q_\mu, p_\mu^\alpha, Q_\mu^{\alpha\beta}) = (q_x, q_y, p_x^x, p_x^y, p_x^z, p_y^x, p_y^y, p_y^z, Q_x^{xx}, Q_x^{xy}, \dots)$. Hence m_u, m_v denote unknown multipole coefficients. Quantities a_{uv} arise from the bulk energy, for example,

$$a_{11(q_xq_x)} \propto \int_V dV r^{-4},$$
$$a_{33(p_x^x p_x^x)} \propto \int_V dV r^{-6},$$
$$a_{15(q_x p_x^z)} \propto \int_V dV z r^{-6},$$

etc. Apparently, all a_{uu} are positive and not equal to zero, and a_{uv} depend on the particle shape. Each c_u is the sum of two terms c_u^p and c_u^a arising from the polar and azimuthal anchoring, respectively, $c_u = c_u^p + c_u^a$. So, for instance,

$$c_{1(q_x)}^p \propto \oint dS\, W^p\nu_z\nu_x, \quad c_{1(q_x)}^a \propto -\oint dS\, W^a\tau_z\tau_x,$$
$$c_{3(p_x^x)}^p \propto \oint dS\, W^p\nu_z\nu_x s_x, \quad c_{3(p_x^x)}^a \propto -\oint dS\, W^a\tau_z\tau_x s_x.$$

c_u depends on both the anchoring and the particle's shape, and $\mathbf{s} = (s_x, s_y, s_z)$ is the radius vector from the center of the particle to the point **s** at the surface [this center of the particle coincides with the center of the coordinate system (CS) from which all r_α are measured].

Now it is natural to assume that the system under investigation is in equilibrium. Therefore, its energy is minimal. Hence one can find the multipole coefficients from the following system of linear equations, $\frac{\partial F_{\text{harm}}}{\partial m_u} = 0$:

$$a_{uu}m_u + \sum_{v,v\neq u} a_{uv}m_v + c_u = 0, \tag{25}$$

or the same in the matrix form:

$$\hat{A}\mathbf{m} = -\mathbf{c}. \tag{26}$$

Here we should make some remarks. First of all, this equation (26) is the exact equation for the multipole coefficients $\mathbf{m}$ for the weak anchoring case. In this case, we know exactly the weak anchoring coefficient $W_{a,p}(\mathbf{s})$ and vector fields $\boldsymbol{\nu}(\mathbf{s}),\boldsymbol{\tau}(\mathbf{s})$, we can calculate all c_u and a_{uv}, and finally we can solve this matrix equation and find all 18 unknown coefficients.

On the other hand, this long procedure is usually unnecessary. Usually we do not need to calculate coefficients $\mathbf{m}$—we can measure them in the experiment. It is much more valuable just to understand which coefficients vanish and which remain nonzero. If we know this, we can find nonzero coefficients from the fitting of the experimental data. So the main strategy is to understand which coefficients vanish and which remain nonzero *without solving the system* (26) *on the basis of just symmetry considerations*.

From this strategy point of view, the strong anchoring case can be considered as well. When the anchoring strength on the real surface of the particle is strong ($\text{Wr}_0/K > 1$), usually topological defects arise in the vicinity. We can put all of them into the area called the coat [31], which has the same symmetry elements as the director field itself. The deformations are small beyond the coat. This means that we can put some distribution $W_{a,p}(\mathbf{s}),\boldsymbol{\nu}(\mathbf{s}),\boldsymbol{\tau}(\mathbf{s})$ on the surface of the coat, which matches with the director symmetry. Inasmuch as this distribution is unknown exactly, we cannot calculate c_u exactly and we cannot find exact values of the multipole coefficients $\mathbf{m}$ in this case. But we do not need this. We just need to know which coefficients $\mathbf{m}$ are nonzero based on the symmetry of the coat without solving (26). This strategy is realized in the next subsections.

Since $\mathbf{c} = \mathbf{c}^p + \mathbf{c}^a$, a solution of the system (26) can be written as the sum

$$\mathbf{m} = \mathbf{m}^p + \mathbf{m}^a \tag{27}$$

of two solutions of the following systems:

$$\hat{A}\mathbf{m}^p = -\mathbf{c}^p, \tag{28}$$

$$\hat{A}\mathbf{m}^a = -\mathbf{c}^a. \tag{29}$$

Thus the polar and azimuthal anchorings make their contributions to the coefficients independently and we can consider these two cases separately.

A. Polar anchoring

Suppose that we have a particle with usual polar anchoring on its surface, $W^a \equiv 0$. Then the multipole coefficients satisfy system (28). Here we should say that the phrase "particle symmetry" means that the appropriate symmetry element belongs to the particle shape as well as to the anchoring distribution $W^p(\mathbf{s})$. Thus, in terms of symmetry, particles of symmetrical shape with asymmetric anchoring do not differ from those of asymmetrical shape with symmetric $W^p(\mathbf{s})$.

Assume first that the particle has one plane of symmetry. Say, for instance, that it coincides with the coordinate xz plane. Then for any point $\mathbf{s} = (x,y,z)$, where $\boldsymbol{\nu} = (\nu_x,\nu_y,\nu_z)$, there exists point $\mathbf{s}' = (x,-y,z)$, where $\boldsymbol{\nu} = (\nu_x,-\nu_y,\nu_z)$, and $W^p(\mathbf{s}) = W^p(\mathbf{s}')$. Then using these symmetry relations, one can easily ensure that, for example, $a_{q_xq_x} = K\int dV r^{-4} \neq 0$, $a_{q_xp_x^y} = 4K\int dV y r^{-6} = 0$, $c^p_{q_y} = 2\int dS\, W^p \nu_z \nu_y s^{-1} = 0$, etc. In the same way, $a_{q_xp_x^y} = a_{p_x^yp_x^y} = a_{p_x^yp_x^z} = a_{q_yp_y^y} = a_{p_y^xp_y^y} = a_{p_y^yp_y^z} = 0$ and $c^p_{q_y} = c^p_{p_y^x} = c^p_{p_y^z} = c^p_{p_x^y} = 0$. It is well known that if the leading term in n_μ decreases as r^{-n}, then the leading anharmonic correction will fall off as r^{-3n} [29]. Thus, quadrupolar terms can be neglected here as anharmonic corrections to n_μ. Since in vector $\mathbf{m}$ the multipole coefficients can be arranged in any order, we are able to rewrite the system (25) in the following matrix form $\hat{A}\mathbf{m}^p = -\mathbf{c}^p$:

$$\begin{pmatrix}
a_{q_x} & b_{q_xp_x^x} & b_{q_xp_x^z} & 0 & 0 & 0 & 0 & 0\\
b_{q_xp_x^x} & a_{p_x^x} & b_{p_x^xp_x^z} & 0 & 0 & 0 & 0 & 0\\
b_{q_xp_x^z} & b_{p_x^xp_x^z} & a_{p_x^z} & 0 & 0 & 0 & 0 & 0\\
0 & 0 & 0 & a_{p_y^y} & 0 & 0 & 0 & 0\\
0 & 0 & 0 & 0 & a_{p_x^y} & 0 & 0 & 0\\
0 & 0 & 0 & 0 & 0 & a_{q_y} & b_{q_yp_y^x} & b_{q_yp_y^z}\\
0 & 0 & 0 & 0 & 0 & b_{q_yp_y^x} & a_{p_y^x} & b_{p_y^xp_y^z}\\
0 & 0 & 0 & 0 & 0 & b_{q_yp_y^z} & b_{p_y^xp_y^z} & a_{p_y^z}
\end{pmatrix}
\times
\begin{pmatrix} q_x\\ p_x^x\\ p_x^z\\ p_y^y\\ p_x^y\\ q_y\\ p_y^x\\ p_y^z \end{pmatrix}
= -
\begin{pmatrix} c^p_{q_x}\\ c^p_{p_x^x}\\ c^p_{p_x^z}\\ c^p_{p_y^y}\\ 0\\ 0\\ 0\\ 0 \end{pmatrix}, \tag{30}$$

Here $\hat{A}$ is a block-diagonal matrix, $\hat{A} = \begin{pmatrix} \hat{A}_{nh} & 0\\ 0 & \hat{A}_h \end{pmatrix}$. So the system (25) splits into two independent subsystems, nonhomogeneous with matrix $\hat{A}_{nh}$ and homogeneous with matrix $\hat{A}_h$. At the same time, $\hat{A}$ is a positive-definite matrix. Indeed, we can treat the components of arbitrary nonzero vector $\mathbf{m}$ as the coefficients of some multipole expansion, and then

$$\mathbf{m}^T\hat{A}\mathbf{m} = K\int dV(\nabla n_\mu)^2 > 0. \tag{31}$$

Thus $\det\hat{A} = \det\hat{A}_{nh}\det\hat{A}_h > 0$. So the homogeneous subsystem has only a trivial solution. It is easy to ensure that the same scenario occurs for particles of other symmetries. If certain c^p_u is equal to zero, then the related multipole coefficient m_u vanishes: $c^p_u = 0 \Rightarrow m^p_u = 0$.

Accordingly, only those multipole coefficients can exist which are allowed by the particle symmetry from the Table I.

Note that the same classification was obtained in Ref. [31] on the basis of gradient expansion ∂n_μ in the center of the particle. But actually the gradient expansion cannot be done

TABLE I. Multipole coefficients and symmetry of the shape. σ_{ik} means that the particle's plane of symmetry coincides with the coordinate ik plane, and $\mathcal{I}$ denotes the inversion center. If a colloidal particle has at least one of the inhibiting symmetry elements, then the appropriate multipole coefficient vanishes.

Defining integral	Multipole coefficient	Inhibiting symmetry	Multipole coefficient	Inhibiting symmetry
$\oint dS\, W^p \nu_z \nu_\mu$	q_x	σ_{xy}, σ_{yz}	q_y	σ_{xy}, σ_{xz}
$\oint dS\, W^p \nu_z \nu_\mu x$	p_x^x	σ_{xy}, $\mathcal{I}$	p_y^x	σ_{xy}, σ_{xz}, σ_{yz}, $\mathcal{I}$
$\oint dS\, W^p \nu_z \nu_\mu y$	p_x^y	σ_{xy}, σ_{xz}, σ_{yz}, $\mathcal{I}$	p_y^y	σ_{xy}, $\mathcal{I}$
$\oint dS\, W^p \nu_z \nu_\mu z$	p_x^z	σ_{yz}, $\mathcal{I}$	p_y^z	σ_{xz}, $\mathcal{I}$
$\oint dS\, W^p \nu_z \nu_\mu xx$	Q_x^{xx}	σ_{xy}, σ_{yz}	Q_y^{xx}	σ_{xy}, σ_{xz}
$\oint dS\, W^p \nu_z \nu_\mu yy$	Q_x^{yy}	σ_{xy}, σ_{yz}	Q_y^{yy}	σ_{xy}, σ_{xz}
$\oint dS\, W^p \nu_z \nu_\mu zz$	Q_x^{zz}	σ_{xy}, σ_{yz}	Q_y^{zz}	σ_{xy}, σ_{xz}
$\oint dS\, W^p \nu_z \nu_\mu xy$	Q_x^{xy}	σ_{xz}, σ_{xy}	Q_y^{xy}	σ_{xy}, σ_{yz}
$\oint dS\, W^p \nu_z \nu_\mu xz$	Q_x^{xz}		Q_y^{xz}	σ_{xz}, σ_{yz}
$\oint dS\, W^p \nu_z \nu_\mu yz$	Q_x^{yz}	σ_{yz}, σ_{xz}	Q_y^{yz}	

exactly as $\partial n_\mu \approx 1$ is not a small parameter. Therefore, the current approach can be considered as more consistent and correct.

Here we should remark that multipole coefficients $\mathbf{m}$ depend on the chosen coordinate system. In one coordinate system CS1, there will be one set of parameters $\mathbf{m}_1$, and in CS2 (which can be rotated or shifted by some vector $\mathbf{d}$ with respect to CS1) there will be another set of multipole coefficients $\mathbf{m}_2$, but the total sum (4) will be the same in both CSs. In our consideration, we have chosen the most appropriate case when symmetry planes coincide with coordinate planes, as in this CS the classification is possible and useful. But in any CS the main multipole coefficient q_μ will be the same as well as in electrostatics—the charge does not depend on the CS [45], while high-order moments do depend on the CS.

B. Azimuthal anchoring and possible chirality of the colloidal particles

As follows from (27) and (29), the long-ranged director deformations can also arise from the azimuthal anchoring of NLC molecules on the particle surface.

Simple examples of such particles are uniaxial helicoids—axially symmetric particles like cylinders or cones with the helicoidal alignment along their easy axes z (see Figs. 1 and 2). For this case, we need to take $W^a > 0$, and vector $\tau(\mathbf{s})$ makes screw thread at the surface of the particle. Then using the method suggested in the previous subsection, one can find that multipole coefficients $\mathbf{m}^a$ in this case are defined from Table II. Inasmuch as $p_{\rm hel} \propto \oint dS\, W^a \tau_z \tau_y x$ and $Q_{\rm hel} \propto \oint dS\, W^a \tau_z \tau_y xz$, then $p_{\rm hel} > 0$ and $Q_{\rm hel} > 0$ for right-handed helicity and $p_{\rm hel} < 0$ and $Q_{\rm hel} < 0$ for left-handed helicity (see Fig. 1).

1. *Interaction between helicoid cylinders*

Consider cylinders (or other symmetric particles such as ellipsoids or spheres) with helicoidal alignment at the surface (see Fig. 1). This azimuthal helicoid anchoring gives rise to nonzero dipole moments $p_y^x = p_{\rm hel} = -p_x^y$, though the shape of the cylinder does not produce any dipole moments (see Table I). Then substitution into (11) gives the dipole-dipole elastic interaction between helicoid cylinders (ellipsoids or spheres):

$$U_{\rm dd} = -4\pi K p_{\rm hel} p'_{\rm hel} [\partial_x \partial'_x G_y(\mathbf{x},\mathbf{x}') + \partial_y \partial'_y G_x(\mathbf{x},\mathbf{x}')]. \quad (32)$$

The Green's functions $G_x \neq G_y$ are different only when some external field (electric or magnetic) is applied along the axis x or y [42]. When the external fields are absent in any other cases (as in homeotropic or planar nematic cells),

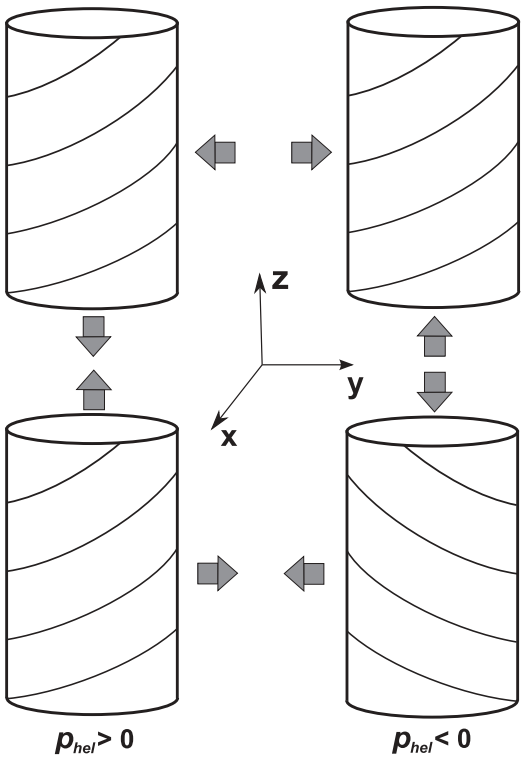

FIG. 1. Helicoid cylinders with the same handedness $p_{\rm hel} p'_{\rm hel} > 0$ attract along the z axis and repel in a perpendicular direction and vice versa for helicoids with different handedness $p_{\rm hel} p'_{\rm hel} < 0$ [see (34)].

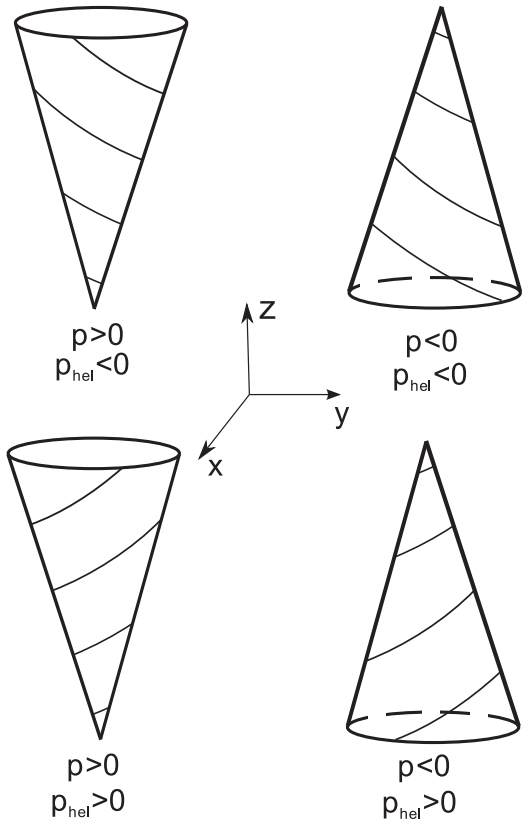

FIG. 2. Helicoid cones with different dipole moments p and $p_{\rm hel}$ produced by shape and azimuthal helical anchoring, respectively [see (38)].

$G_x = G_y = G$ and we come to the expression

$$U_{\rm dd} = -4\pi K p_{\rm hel} p'_{\rm hel} \partial_\mu \partial'_\mu G(\mathbf{x},\mathbf{x}'), \tag{33}$$

which coincides with the dipole-dipole interaction between usual axially symmetric dipole particles ($\partial_\mu \partial'_\mu = \partial_x \partial'_x + \partial_y \partial'_y$). In the bulk nematic liquid crystal, for example,

TABLE II. Multipole coefficients which are born by azimuthal helical alignment along the z axis. $p_{\rm hel} > 0$ and $Q_{\rm hel} > 0$ for right-handed helicity and $p_{\rm hel} < 0$ and $Q_{\rm hel} < 0$ for left-handed helicity (see Fig. 1).

Defining integral	Multipole coefficient	Value	Multipole coefficient	Value
$\oint dS\ W^a \tau_z \tau_\mu$	q_x	0	q_y	0
$\oint dS\ W^a \tau_z \tau_\mu x$	p_x^x	0	p_y^x	$p_{\rm hel}$
$\oint dS\ W^a \tau_z \tau_\mu y$	p_x^y	$-p_{\rm hel}$	p_y^y	0
$\oint dS\ W^a \tau_z \tau_\mu z$	p_x^z	0	p_y^z	0
$\oint dS\ W^a \tau_z \tau_\mu xx$	Q_x^{xx}	0	Q_y^{xx}	0
$\oint dS\ W^a \tau_z \tau_\mu yy$	Q_x^{yy}	0	Q_y^{yy}	0
$\oint dS\ W^a \tau_z \tau_\mu zz$	Q_x^{zz}	0	Q_y^{zz}	0
$\oint dS\ W^a \tau_z \tau_\mu xy$	Q_x^{xy}	0	Q_y^{xy}	0
$\oint dS\ W^a \tau_z \tau_\mu xz$	Q_x^{xz}	0	Q_y^{xz}	$Q_{\rm hel}$
$\oint dS\ W^a \tau_z \tau_\mu yz$	Q_x^{yz}	$-Q_{\rm hel}$	Q_y^{yz}	0

$G(\mathbf{x},\mathbf{x}') = \frac{1}{|\mathbf{x}-\mathbf{x}'|}$ so that

$$U_{\rm dd}^{\rm bulk} = 4\pi K p_{\rm hel} p'_{\rm hel} \frac{(1-3\cos^2\theta)}{r^3}, \tag{34}$$

where θ is the angle between $\mathbf{r}$ and z, and the director field around the particle has the form

$$n_x = -p_{\rm hel}\frac{y}{r^3}, \quad n_y = p_{\rm hel}\frac{x}{r^3}. \tag{35}$$

The formula (34) means that helicoids with the same handedness $p_{\rm hel} p'_{\rm hel} > 0$ attract along the z axis and repel in a perpendicular direction and vice versa for helicoids with different handedness $p_{\rm hel} p'_{\rm hel} < 0$ (see Fig. 1). In the nematic cell, the interaction, falling off as r^{-3} in the bulk NLC, becomes exponentially screened at distances comparable to the thickness L of the cell. At the same time, the borders between the attraction and repulsion zones transform from straight lines into some parabola-like curves. These effects are caused only by the confining walls, so they do not depend on the particle shape and anchoring. More detailed consideration of these issues is presented in Refs. [40,41].

2. *Interaction between helicoid cones*

Consider cones (or other axially symmetric particles without symmetry plane σ_{xy}) with helicoidal alignment at the surface (see Fig. 2). The shape of the particle produces dipole moments $p_x^x = p_y^y = p$ according to Table I. Azimuthal helicoid anchoring gives rise to nonzero dipole moments $p_y^x = p_{\rm hel} = -p_x^y$. Then substitution of it into (11) gives the dipole-dipole elastic interaction between helicoid cones:

$$\begin{aligned} U_{\rm dd} = -4\pi K \{ & pp' [\partial_x \partial'_x G_x(\mathbf{x},\mathbf{x}') + \partial_y \partial'_y G_y(\mathbf{x},\mathbf{x}')] \\ & + p_{\rm hel} p'_{\rm hel} [\partial_x \partial'_x G_y(\mathbf{x},\mathbf{x}') + \partial_y \partial'_y G_x(\mathbf{x},\mathbf{x}')] \}. \end{aligned} \tag{36}$$

In the absence of the external fields, $G_x = G_y = G$ and we come to the expression

$$U_{\rm dd} = -4\pi K (pp' + p_{\rm hel} p'_{\rm hel}) \partial_\mu \partial'_\mu G(\mathbf{x},\mathbf{x}'). \tag{37}$$

In the confined nematic, this formula gives the same results as in the [41] but with a new coefficient $pp' + p_{\rm hel} p'_{\rm hel}$.

In the bulk nematic liquid crystal, $G(\mathbf{x},\mathbf{x}') = \frac{1}{|\mathbf{x}-\mathbf{x}'|}$, so that

$$U_{\rm dd}^{\rm bulk} = 4\pi K (pp' + p_{\rm hel} p'_{\rm hel}) \frac{(1-3\cos^2\theta)}{r^3}, \tag{38}$$

and the director field around the particle has the form

$$n_x = p\frac{x}{r^3} - p_{\rm hel}\frac{y}{r^3}, \quad n_y = p\frac{y}{r^3} + p_{\rm hel}\frac{x}{r^3}. \tag{39}$$

Formulas similar to (34), (35), (38), and (39) were first obtained in Ref. [34], but our results predict three times stronger interaction. In Ref. [34], the authors made a very good classification of different types of dipoles in nematostatics based on the firm fixation of the director field on the surface of the imaginary sphere enclosing the particle and containing all the defects inside. At first glance, it seems quite similar to the coat approach used above. The authors of [34] do not use any anchoring surface energy explicitly and consider the total energy as just the bulk one. But the total energy is the sum of the bulk and surface energies. This, we suppose, is the reason for the discrepancy. The surface terms do play an important

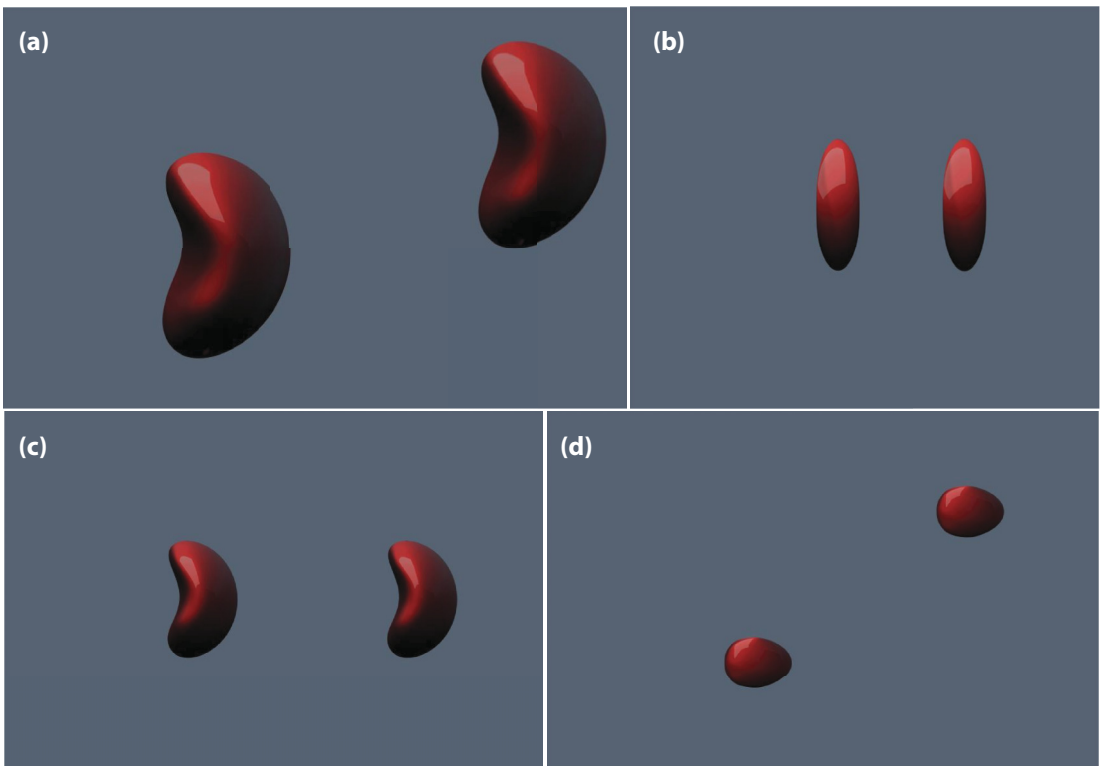

FIG. 3. (Color online) (a) General banana-shaped particles, (b) front view (see Figs. 5 and 8), (c) side view (see Fig. 4), (d) top view (see Fig. 9).

role and increase the energy of the system, and they should be taken into consideration. In the current approach, the surface terms are taken into account via the terms $-4\pi q_\mu(\mathbf{x})n_\mu - 4\pi p_\mu^\alpha(\mathbf{x})\partial_\alpha n_\mu - 4\pi Q_\mu^{\alpha\beta}(\mathbf{x})\partial_\alpha\partial_\beta n_\mu$ in the effective free energy (6). These terms in the effective free energy (6) replace surface terms in the real free energy (22) so they can be effectively considered as surface-born.

IV. BANANA-SHAPED PARTICLES IN NEMATIC CELLS

As an example of the interaction between nonaxially symmetric colloids, we consider now the interaction between banana-shaped particles (see Fig. 3). Here let us content ourselves with the dipole-dipole interactions in homeotropic and planar nematic cells.

A. Homeotropic cell

A coordinate system for this case is depicted in Figs. 4(a) and 4(b). The Green's function then has a form that is well known in electrostatics [45],

$$G_\mu(\mathbf{x},\mathbf{x}') = \frac{4}{L}\sum_{n=1}^{\infty}\sum_{m=-\infty}^{\infty} e^{im(\varphi-\varphi')}\sin\frac{n\pi z}{L}\sin\frac{n\pi z'}{L} \times I_m(\lambda_n\rho_<)K_m(\lambda_n\rho_>), \tag{40}$$

where I_m, K_m are modified Bessel functions, $\tan\varphi = \frac{y}{x}$, $\tan\varphi' = \frac{y'}{x'}$, $\lambda_n = \frac{n\pi}{L}$, and $\rho_<$ is the smaller of $\rho = \sqrt{x^2+y^2}$ and $\rho' = \sqrt{x'^2+y'^2}$.

Every banana-shaped particle has two orthogonal symmetry planes. Suppose first that the particles are oriented in such a way that these planes are parallel to the coordinate xz and yz planes [see Fig. 4(a)], i.e., particles are located primarily perpendicular to the director (we will use the symbol $\perp$ for this case). Then using Table I, one can easily find that the allowed dipole coefficients are p_x^x and p_y^y. Below we omit the upper indexes and assume $p_y > p_x$. Note that $p_x = p_y$ for axially symmetric particles. It follows from (14) that

$$U_{\mathrm{dd},\perp}^{\mathrm{hom}} = -4\pi K[p_x p_x'\partial_x\partial_x' G + p_y p_y'\partial_y\partial_y' G], \tag{41}$$

$$U_{\mathrm{dd},\perp}^{\mathrm{hom}} = \frac{8\pi K}{L}[(p_x p_x' + p_y p_y')A_1 + (p_x p_x' - p_y p_y')A_2\cos 2\phi], \tag{42}$$

where $\rho = \sqrt{(y-y')^2+(x-x')^2}$ is the horizontal projection of the distance between particles, ϕ is the azimuthal angle between ρ and the x axis,

$$A_1 = \sum_{n=1}^{\infty}\lambda_n^2\sin\frac{n\pi z}{L}\sin\frac{n\pi z'}{L}K_0(\lambda_n\rho), \tag{43}$$

$$A_2 = \sum_{n=1}^{\infty}\lambda_n^2\sin\frac{n\pi z}{L}\sin\frac{n\pi z'}{L}K_2(\lambda_n\rho). \tag{44}$$

We see that axially symmetric particles either attract or repel each other everywhere inside the homeotropic cell, while the dipole-dipole interaction between banana-shaped particles is anisotropic. Before proceeding to a discussion of this interaction in the cell, let us consider its features in the bulk liquid crystal. The Green's function for the bulk NLC

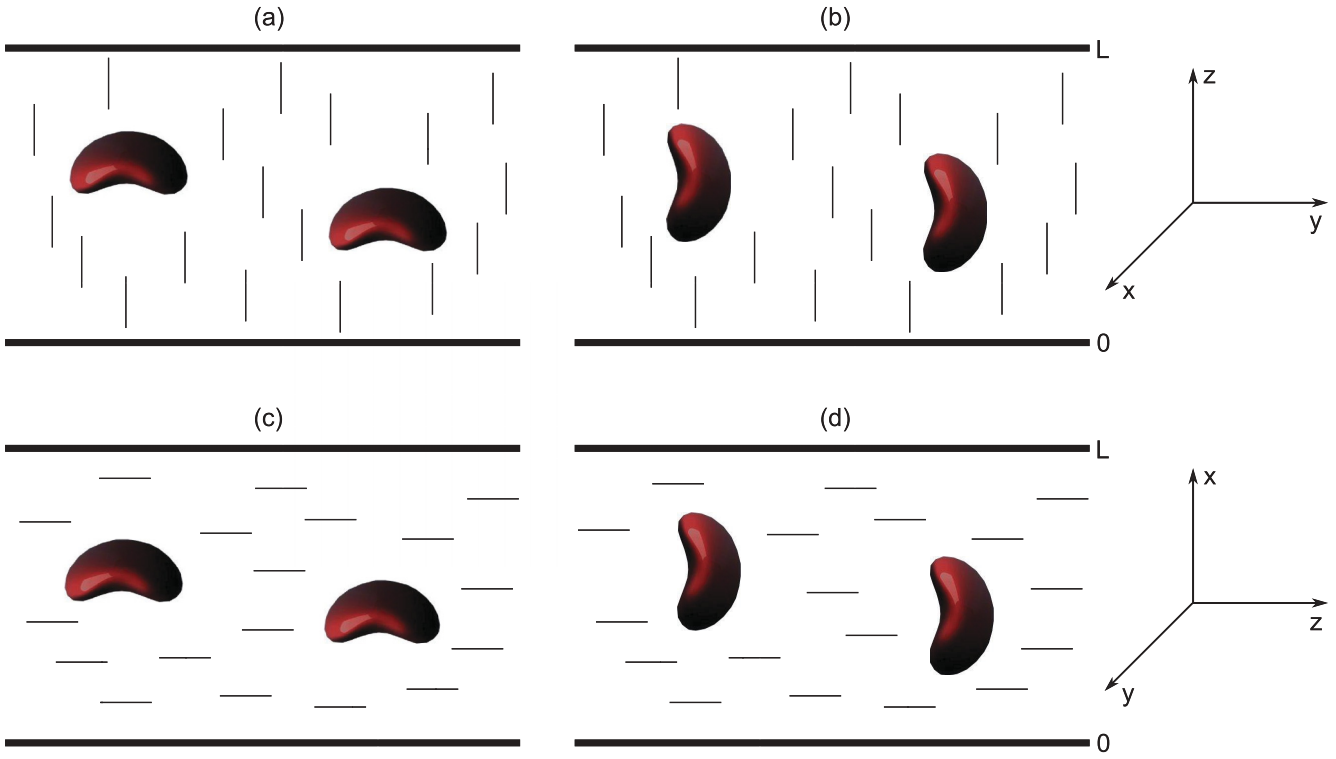

FIG. 4. (Color online) Banana-shaped particles in the nematic cell, side view (see Fig. 3 as well).

is $G(\mathbf{x},\mathbf{x}') = \frac{1}{|\mathbf{x}-\mathbf{x}'|}$ so that $U^{\rm bulk}_{{\rm dd},\perp}$ is anisotropic as well,

$$U^{\rm bulk}_{{\rm dd},\perp} = -\frac{4\pi K}{r^3}[p_x p'_x + p_y p'_y - 3\sin^2\theta(p_x p'_x \cos^2\phi + p_y p'_y \sin^2\phi)], \qquad (45)$$

where r is the distance between particles, θ is the polar angle between $\mathbf{r}$ and the z axis, and ϕ is the azimuthal angle between ρ and the x axis. Note that a similar formula for bulk NLC was obtained in Ref. [34], but our result predicts three times stronger interaction. A map of the attraction and repulsion zones between two particles with $z = z'$ in the infinite crystal is depicted by the dashed lines in Fig. 5.

Now assume that the particles are located in the center of the homeotropic cell $z = z' = \frac{L}{2}$ (solid lines in Fig. 5). At small distances $\rho \ll L$, the interaction is the same as in the bulk nematic $U^{\rm hom}_{{\rm dd},\perp} \to U^{\rm bulk}_{{\rm dd},\perp}$. But as ρ increases, the lateral zones become closed. So identical particles attract inside some dumbbell-shaped regions along the x axis when $p_y > \sqrt{2}p_x$. These regions shrink as $|p_y - \sqrt{2}p_x|$ decreases and collapse to the point when $p_y = \sqrt{2}p_x$.The crossover from the attraction to the repulsion when both particles are located along the x axes and $p_y > \sqrt{2}p_x$ is shown in Fig. 6.

When $\frac{p_x}{\sqrt{2}} < p_y < \sqrt{2}p_x$, there will be only repulsion for every ϕ in the perpendicular plane $\theta = \pi/2$. When $p_y < \frac{p_x}{\sqrt{2}}$, there will be attraction inside some dumbbell-shaped regions along the y axis and repulsion everywhere along the x axis.

Another important issue is the energy dependence on the distance between particles. It follows from (45) that in the bulk nematic host, the interaction of dipolar colloidal particles decreases as ρ^{-3} (see the dashed line 4 in Fig. 7). But in the cell we see a completely different picture. The interaction potential

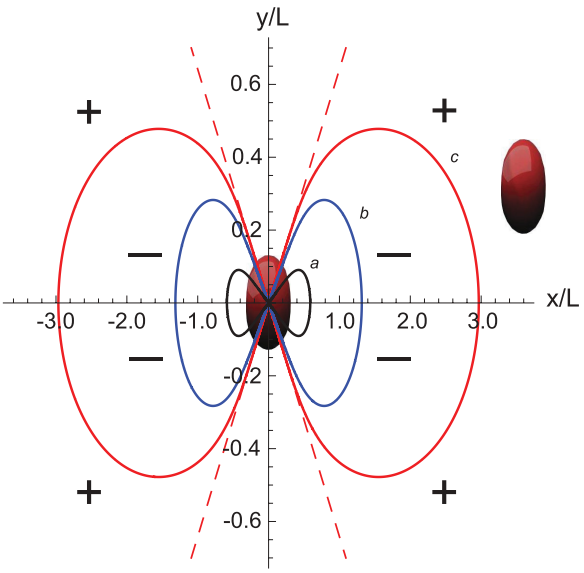

FIG. 5. (Color online) Map of the attraction and repulsion zones for two identical banana-shaped particles, $p_x = p'_x$ and $p_y = p'_y = \alpha p_x$, $\alpha > \sqrt{2}$, according to (42). Black line (a) corresponds to the case $p_y = 1.5p_x$, blue line (b) corresponds to the $p_y = 2p_x$, and red line (c) corresponds to the $p_y = 3p_x$. The particles are located in the center of the homeotropic cell $z = z' = \frac{L}{2}$. Their orientations are shown in Figs. 3(b) and 4(a). The sign "–" means attraction (inside of the dumbbell-shaped regions), and "+" means repulsion. If $p_y < \frac{p_x}{\sqrt{2}}$, then the attraction will appear along the y axis.

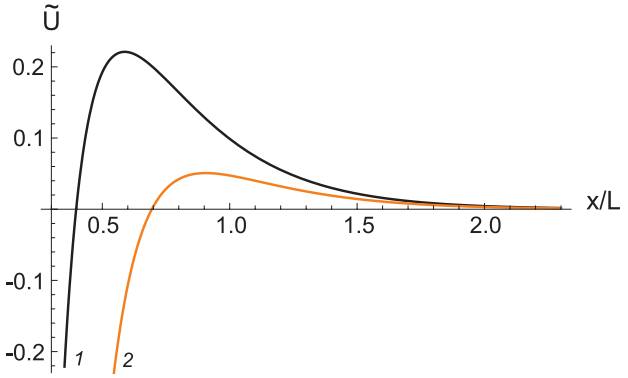

FIG. 6. (Color online) The crossover from the attraction to the repulsion between two banana-shaped particles located in the middle of the homeotropic cell $z = z' = \frac{L}{2}$ along the x axis [see Figs. 4(a) and 5], $p_x = p'_x$, $p_y = p'_y = \alpha p_x$ for $\alpha > \sqrt{2}$. $\tilde{U} = U^{\rm hom}_{{\rm dd},\perp} L^3/8\pi K(p_x p'_x + p_y p'_y)$, where $U^{\rm hom}_{{\rm dd},\perp}$ is given by (42) and $\phi = 0$. Solid black line 1 corresponds to $p_y = p'_y = 1.5 p_x$, orange line 2 corresponds to $p_y = p'_y = 1.7 p_x$.

falls off as ρ^{-3} only when $\rho < L$. At larger distances $\rho > L$, the potential becomes screened by the cell walls (see solid line 2 in Fig. 7). Such screening, known as the confinement effect, was first reported experimentally in Ref. [19] and theoretically explained in Refs. [36,41] for spherical particles. This phenomenon is related only to the confining surfaces and therefore it occurs despite the particle shape.

But the particle orientation examined above is not the only possibility. Their symmetry planes can be parallel to the coordinate yz and xy planes as well [see Fig. 4(b)], i.e., particles lie primarily parallel to the director (we will use $||$ for this case). Then we have one dipole coefficient $p^z_y = p \neq 0$ as

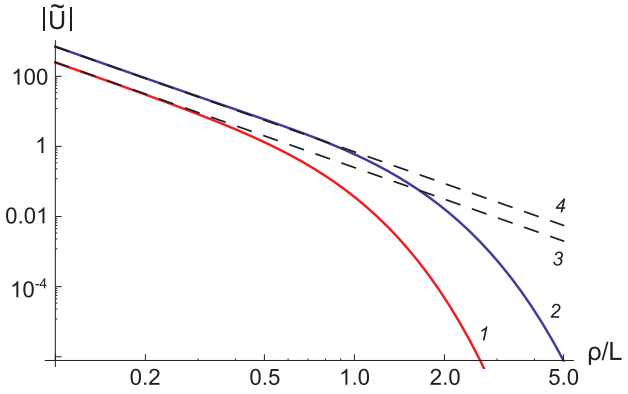

FIG. 7. (Color online) Log-log plot of the dimensionless energy of the dipole-dipole interaction as a function of the distance between two banana-shaped particles located in the middle of the homeotropic cell $z = z' = \frac{L}{2}$. Solid blue line 2 corresponds to the particle repulsion for the orientation along the y axis depicted in Fig. 4(a), $p_x = p'_x$, $p_y = p'_y = 2p_x$, $2\phi = \pi$, and $\tilde{U} = U_{\rm dd} L^3/8\pi K(p_x p'_x + p_y p'_y)$, where $U_{\rm dd} > 0$ is given by (42). Dashed line 4 is an appropriate power-law asymptotic $U^{\rm unc}_{\rm dd} L^3/4\pi K(p_x p'_x + p_y p'_y) \propto (\frac{L}{\rho})^3$. Solid red line 1 corresponds to the particle attraction along the y axis in Fig. 4(b), $p^z_y = p \neq 0$ and $\tilde{U} = U_{\rm dd} L^3/16\pi K p p'$, where $U_{\rm dd} < 0$ is given by (47). Dashed line 3 is the appropriate power-law asymptotic $\frac{1}{4}(\frac{L}{\rho})^3$.

follows from Table I. Thus

$$U^{\rm hom}_{{\rm dd},||} = -4\pi K p p' \partial_z \partial'_z G, \tag{46}$$

$$U^{\rm hom}_{{\rm dd},||} = -\frac{16\pi K p p'}{L} \sum_{n=1}^{\infty} \lambda_n^2 \cos\frac{n\pi z}{L} \cos\frac{n\pi z'}{L} K_0(\lambda_n \rho). \tag{47}$$

As in the previous case, the interaction given by (47) is screened by the cell walls (solid line 1 in Fig. 7). But here it exhibits cylindrical symmetry. In particular, parallel dipoles with $z = z'$ attract each other throughout the cell plane. In the unlimited case, $G = \frac{1}{|\mathbf{x}-\mathbf{x}'|}$ and (47) becomes

$$U^{\rm bulk}_{{\rm dd},||} = -\frac{4\pi K p p'}{r^3}(1 - 3\cos^2\theta). \tag{48}$$

A similar result for the bulk NLC was obtained in Ref. [34], but our result again predicts three times stronger interaction.

B. Planar cell

Let us choose the coordinate system as shown in Figs. 4(c) and 4(d). Then the Green's function is as follows:

$$G_\mu(\mathbf{x},\mathbf{x}') = \frac{4}{L} \sum_{n=1}^{\infty} \sum_{m=-\infty}^{\infty} e^{im(\varphi-\varphi')} \sin\frac{n\pi x}{L} \sin\frac{n\pi x'}{L} \times I_m(\lambda_n \rho_<) K_m(\lambda_n \rho_>), \tag{49}$$

where L is the cell thickness, I_m, K_m are modified Bessel functions, $\tan\varphi = \frac{y}{z}$, $\tan\varphi' = \frac{y'}{z'}$, $\lambda_n = \frac{n\pi}{L}$, and $\rho_<$ is the smaller of $\rho = \sqrt{z^2 + y^2}$ and $\rho' = \sqrt{z'^2 + y'^2}$. This Green's function was already used by the authors of [41] to describe interactions between axially symmetric particles. Their predictions were found to be in good agreement with the experimental data for a wide range of L [20].

Imagine first that the particles are oriented as depicted in Fig. 4(c). Hence every particle has two symmetry elements affecting the multipole coefficient's existence. They are σ_{xz} and σ_{xy}. Therefore, as follows from Table I, director deviations here can be described by the only dipole coefficient $p^z_x = p \neq 0$. Then

$$U^{\rm plan}_{{\rm dd},||} = -4\pi K p p' \partial_z \partial'_z G, \tag{50}$$

$$U^{\rm plan}_{{\rm dd},||} = \frac{8\pi K p p'}{L} \sum_{n=1}^{\infty} \lambda_n^2 \sin\frac{n\pi x}{L} \sin\frac{n\pi x'}{L} \times [K_0(\lambda_n \rho) + K_2(\lambda_n \rho)\cos 2\theta], \tag{51}$$

where $\rho = \sqrt{(y-y')^2 + (z-z')^2}$ is the horizontal projection of the distance between particles, and θ is the angle between ρ and the z axis. As in the homeotropic cell, the particles do not "feel" the cell walls at small distances $U^{\rm plan}_{{\rm dd},||} \to -\frac{4\pi K p p'}{\rho^3}(1 - 3\cos^2\theta)$. But if ρ increases, the interaction falls off exponentially [$K_n(z \to \infty) \propto \frac{e^{-z}}{\sqrt{z}}$] and the borders between zones transform from straight lines into some parabola-like curves (see Fig. 8).

Now suppose that the particle symmetry planes are parallel to the coordinate yz and xz planes [see Fig. 4(d)]. The allowed

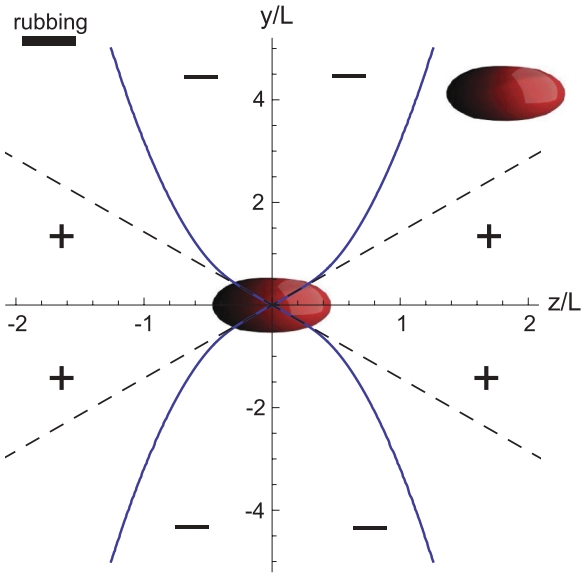

FIG. 8. (Color online) Map of the attraction and repulsion zones for two identical banana-shaped particles, $p = p'$, according to (51). The particles are located in the center of the planar cell $x = x' = \frac{L}{2}$. Their orientation are shown in Figs. 3(b) and 4(c). The sign "–" means attraction, and "+" means repulsion.

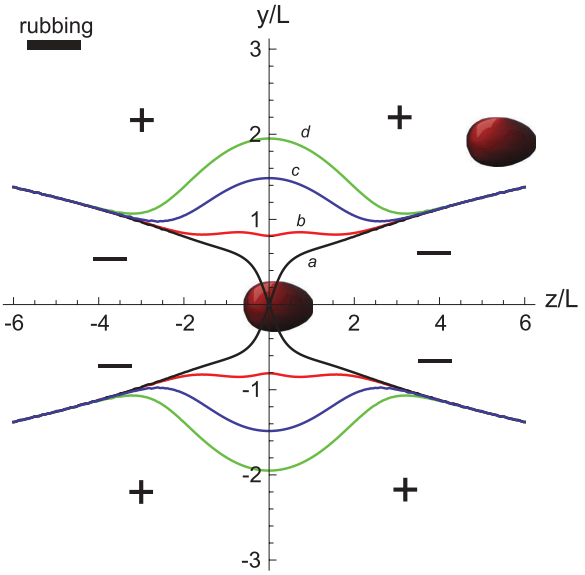

FIG. 9. (Color online) Map of the attraction and repulsion zones for two identical banana-shaped particles $p_x = p'_x$ and $p_y = p'_y$, according to (53). The particles are located in the center of the planar cell $x = x' = \frac{L}{2}$. Their orientations are shown in Figs. 3(d) and 4(d). Black line (a) $p_x = p_y$. Red line (b) $p_x = 2p_y$. Blue line (c) $p_x = 5p_y$. Green line (d) $p_x = 10p_y$. The sign "–" means attraction, and "+" means repulsion.

dipole coefficients are $p_x^x = p_x$ and $p_y^y = p_y$. Thus

$$U_{\mathrm{dd},\perp}^{\mathrm{plan}} = -4\pi K[p_x p'_x \partial_x \partial'_x G + p_y p'_y \partial_y \partial'_y G], \tag{52}$$

$$U_{\mathrm{dd},\perp}^{\mathrm{plan}} = \frac{8\pi K}{L}[-p_x p'_x B_1 + p_y p'_y B_2 - p_y p'_y B_3 \cos 2\theta], \tag{53}$$

where

$$B_1 = 2\sum_{n=1}^{\infty} \lambda_n^2 \cos\frac{n\pi x}{L} \cos\frac{n\pi x'}{L} K_0(\lambda_n \rho), \tag{54}$$

$$B_2 = \sum_{n=1}^{\infty} \lambda_n^2 \sin\frac{n\pi x}{L} \sin\frac{n\pi x'}{L} K_0(\lambda_n \rho), \tag{55}$$

$$B_3 = \sum_{n=1}^{\infty} \lambda_n^2 \sin\frac{n\pi x}{L} \sin\frac{n\pi x'}{L} K_2(\lambda_n \rho). \tag{56}$$

At small distances, $B_1 \to \frac{1}{2}(\frac{L}{\rho})^3$, $B_2 \to \frac{1}{4}(\frac{L}{\rho})^3$, and $B_3 \to \frac{3}{4}(\frac{L}{\rho})^3$ and we come to the fact that in this case $U_{\mathrm{dd}} \to U_{\mathrm{dd}}^{\mathrm{bulk}}$ when $\rho \ll L$ as well. Note that here $U_{\mathrm{dd},\perp}^{\mathrm{bulk}}$ is given by (45) if we set $x = x'$ ($\phi = \pi/2$), that is, $U_{\mathrm{dd},\perp}^{\mathrm{bulk}} = -\frac{4\pi K}{r^3}[p_x p'_x + p_y p'_y - 3p_y p'_y \sin^2\theta]$. Say, for instance, $p_x > p_y$. Then it can be easily found that the interaction between such particles in the bulk nematic is completely repulsive or attractive. In the cell we again have both attraction and repulsion (see Fig. 9). In turn, since the summation in Eq. (54) starts from $n = 2$, B_1 falls off faster than B_2 and B_3. Therefore, when $\rho \gg L$ the interaction is determined only by the coefficients p_y and p'_y. Due to this fact, at large distances these particles will interact as axially symmetrical ones (black lines in Fig. 9). In the same way, if we set $p_y > p_x$, no attraction will appear along the y axis. The map of the interaction in this case will be quite similar to that for the axially symmetrical particles.

V. MONOPOLE-MONOPOLE INTERACTION IN NEMATIC CELLS

Finally, it is worth noting that the elastic monopoles do not "feel" the cell type. Indeed, suppose that we have two ellipsoidal particles suspended in the cell (Fig. 10). Let us assume that their long axes make angles ω and ω' with $\mathbf{n}_0$, $0 < \omega, \omega' < \frac{\pi}{2}$ and they lie in the plane of the figure. This configuration can be achieved with the help of some external electric or magnetic field if particles have a dipole

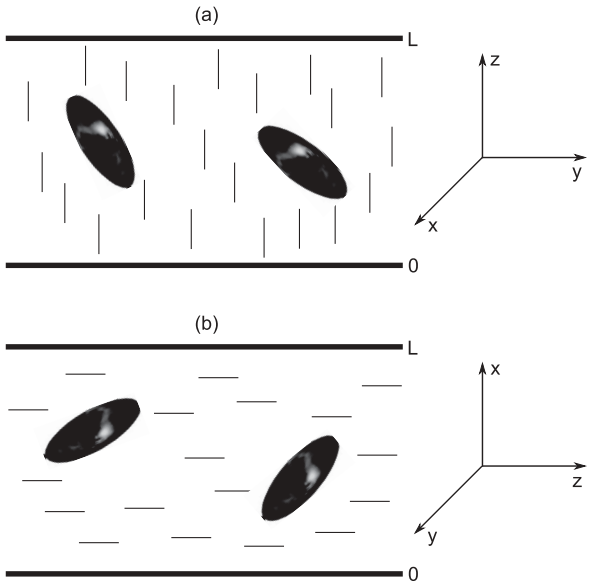

FIG. 10. Ellipsoidal particles in the homeotropic (a) and planar (b) nematic cell.

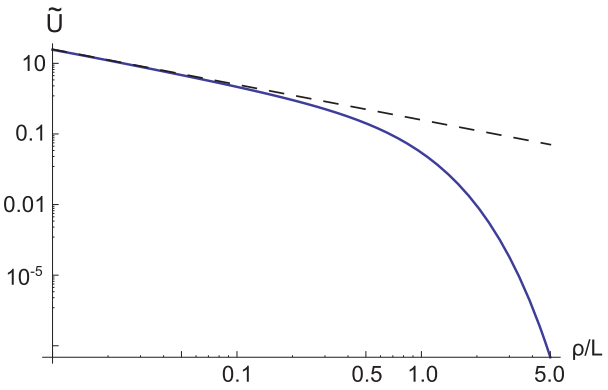

FIG. 11. (Color online) Monopole-monopole interaction in a nematic cell. Elastic monopoles do not "feel" the type of cell. Blue line 1 corresponds to $\tilde{U} = -U_{qq}^{plan} L/16\pi K q q'$. Here U_{qq}^{plan} is given by (58). The dashed line 2 is the Coulomb-like $\tilde{U} = \frac{1}{4\rho/L}$ asymptotics for $\rho \ll L$.

electric or magnetic moment. Since ellipsoids have a center of symmetry, the main deformations produced by these particles are elastic monopoles: $q_x = q'_x = 0, q_y = q, q'_y = q'$ in the homeotropic and $q_x = q$, $q'_x = q', q_y = q'_y = 0$ in the planar cell (see Table I). Then as follows from (40) and (11), the monopole-monopole interaction in the homeotropic cell is given by

$$U_{qq}^{hom} = -\frac{16\pi K q q'}{L} \sum_{n=1}^{\infty} \sin\frac{n\pi z}{L} \sin\frac{n\pi z'}{L} K_0(\lambda_n \rho), \qquad (57)$$

where $\rho = \sqrt{(y-y')^2 + (x-x')^2}$. In the same way, we can find from (49) and (11) that in the planar cell this interaction is described by

$$U_{qq}^{plan} = -\frac{16\pi K q q'}{L} \sum_{n=1}^{\infty} \sin\frac{n\pi x}{L} \sin\frac{n\pi x'}{L} K_0(\lambda_n \rho), \qquad (58)$$

where $\rho = \sqrt{(y-y')^2 + (z-z')^2}$. Expressions (57) and (58) demonstrate that the monopole-monopole interaction is the same and does not depend on the type of the nematic cell (see Fig. 11), as z in Fig. 10(a) is the same as x in Fig. 10(b). For small distances $\rho \ll L$, both (57) and (58) converge to the Coulomb-like law $U_{qq} = -4\pi K q q' \frac{1}{r}$ (see Fig. 11). Equal elastic charges attract, opposite charges repel.

VI. CONCLUSIONS

Colloidal particles suspended in a nematic liquid crystal host cause deviations of the director from its ground state. Far from any particle, these distortions can be written in a form of the multipole expansion.

We develop the method proposed in Ref. [40] for theoretical investigation of elastic interactions between colloidal particles of arbitrary shape and anchoring strength in the confined nematic liquid crystal. General expressions for six different types of multipole elastic interactions are obtained in the confined NLC: monopole-monopole (Coulomb-type), monopole-dipole, monopole-quadrupole, dipole-dipole, dipole-quadrupole, and quadrupole-quadrupole interactions. The obtained formulas remain valid in the presence of the external electric or magnetic fields. The particles with both polar and azimuthal helicoid anchoring are considered. It is found that azimuthal helicoid anchoring and usual polar anchoring produce multipole coefficients independently. In the weak anchoring case, $\mathrm{Wr}_0 < K$, the method proposed enables us to find exact values of all the multipole coefficients. When the anchoring is strong, $\mathrm{Wr}_0 > K$, we cannot find exact values of them, but it is possible to predict which coefficients vanish and which remain nonzero on the basis of the symmetry of the director field. The connection between the symmetry of the director field and multipole coefficients is established. Since this symmetry can be easily observed experimentally, the results we present are applicable for particles of arbitrary shapes, sizes, and anchoring strengths.

Dipole-dipole interactions between helicoid cylinders and cones are found in the confined NLC. In addition, the banana-shaped particles in homeotropic and planar nematic cells are considered. It is found that the dipole-dipole interaction between banana-shaped particles differs greatly from the elastic dipole-dipole interaction between the axially symmetrical particles in the nematic cell. The banana-like particle has two planes of symmetry. Obviously in the equilibrium state one of these planes is always perpendicular to the cell walls. The other can be either perpendicular (say orientation A) or parallel (orientation B) to them. Both of these cases are considered in the homeotropic and planar nematic cell. So, for example, in the homeotropic cell the interaction between particles with the orientation A is anisotropic. Two "bananas" attract inside some dumbbell-shaped region. The more asymmetric the particles are, the larger the region of attraction. But as $r \to \infty$, the interaction becomes completely repulsive. At the same time, the interaction between such particles in the bulk nematic LC preserves its sign independent of the distance. In the planar cell, particles with the orientation B as well as the axially symmetric particles interact anisotropically. But the symmetric particles repel along the direction perpendicular to the rubbing while the asymmetric particles attract at small distances.

It is shown that monopoles do not "feel" the type of nematic cell: monopole-monopole interaction turns out to be the same in the homeotropic and planar nematic cell and converges to the Coulomb law as thickness increases, $L \to \infty$.

[1] P. Poulin, H. Stark, T. C. Lubensky, and D. A. Weitz, Science **275**, 1770 (1997).
[2] P. Poulin, V. Cabuil, and D. A. Weitz, Phys. Rev. Lett. **79**, 4862 (1997).
[3] P. Poulin and D. A. Weitz, Phys. Rev. E **57**, 626 (1998).
[4] C. M. Noel, G. Bossis, A.-M. Chaze, F. Giulieri, and S. Lacis, Phys. Rev. Lett. **96**, 217801 (2006).
[5] I. I. Smalyukh, O. D. Lavrentovich, A. N. Kuzmin, A. V. Kachynski, and P. N. Prasad, Phys. Rev. Lett. **95**, 157801 (2005).

[6] I. I. Smalyukh, A. N. Kuzmin, A. V. Kachynski, P. N. Prasad, and O. D. Lavrentovich, Appl. Phys. Lett. **86**, 021913 (2005).

[7] J. Kotar, M. Vilfan, N. Osterman, D. Babič, M. Čopič, and I. Poberaj, Phys. Rev. Lett. **96**, 207801 (2006).

[8] V. G. Nazarenko, A. B. Nych, and B. I. Lev, Phys. Rev. Lett. **87**, 075504 (2001).

[9] I. I. Smalyukh, S. Chernyshuk, B. I. Lev, A. B. Nych, U. Ognysta, V. G. Nazarenko, and O. D. Lavrentovich, Phys. Rev. Lett. **93**, 117801 (2004).

[10] T. Yamamoto, J. Yamamoto, B. I. Lev, and H. Yokoyama, Appl. Phys. Lett. **81**, 2187 (2002).

[11] B. I. Lev, S. B. Chernyshuk, T. Yamamoto, J. Yamamoto, and H. Yokoyama, Phys. Rev. E **78**, 020701 (2008).

[12] B. I. Lev, A. B. Nych, U. Ognysta, D. Reznikov, S. B. Chernyshuk, and V. G. Nazarenko, Pis'ma Zh. Eksp. Teor. Fiz. **75**, 393 (2002) [JETP Lett. **75**, 322 (2002)].

[13] I. Muševic, M. Škarabot, U. Tkalec, M. Ravnik, and S. Žumer, Science **313**, 954 (2006).

[14] M. Škarabot, M. Ravnik, S. Žumer, U. Tkalec, I. Poberaj, D. Babič, N. Osterman, and I. Muševic, Phys. Rev. E **76**, 051406 (2007).

[15] U. Ognysta, A. Nych, V. Nazarenko, I. Muševic, M. Škarabot, M. Ravnik, S. Žumer, I. Poberaj, and D. Babič, Phys. Rev. Lett. **100**, 217803 (2008).

[16] M. Škarabot, M. Ravnik, S. Žumer, U. Tkalec, I. Poberaj, D. Babič, and I. Muševic, Phys. Rev. E **77**, 061706 (2008).

[17] M. Ravnik, M. Škarabot, S. Žumer, U. Tkalec, I. Poberaj, D. Babič, N. Osterman, and I. Muševic, Phys. Rev. Lett. **99**, 247801 (2007).

[18] U. Tkalec, M. Ravnik, S. Žumer, and I. Muševic, Phys. Rev. Lett. **103**, 127801 (2009).

[19] M. Vilfan, N. Osterman, M. Čopič, M. Ravnik, S. Žumer, J. Kotar, D. Babič, and I. Poberaj, Phys. Rev. Lett. **101**, 237801 (2008).

[20] N. Kondo, Y. Iwashita, and Y. Kimura, Phys. Rev. E **82**, 020701(R) (2010).

[21] J. I. Fukuda, H. Stark, M. Yoneya, and H. Yokoyama, Phys. Rev. E **69**, 041706 (2004).

[22] K. M. Aoki, B. I. Lev, and H. Yokoyama, Mol. Cryst. Liq. Cryst. **367**, 537 (2001).

[23] D. Andrienko, M. Tasinkevych, and S. Dietrich, Europhys. Lett. **70**, 95 (2005).

[24] M. Tasinkevych and D. Andrienko, Condens. Matter Phys. **13**, 33603 (2010).

[25] T. Kishita, K. Takahashi, M. Ichikawa, J. I. Fukuda, and Y. Kimura, Phys. Rev. E **81**, 010701(R) (2010).

[26] T. Kishita, N. Kondo, K. Takahashi, M. Ichikawa, J. I. Fukuda, and Y. Kimura, Phys. Rev. E **84**, 021704 (2011).

[27] H. Stark, Eur. Phys. J. B **10**, 311 (1999).

[28] D. Andrienko, M. Tasinkevych, P. Patricio, M. P. Allen, and M. M. Telo da Gama, Phys. Rev. E **68**, 051702 (2003).

[29] T. C. Lubensky, D. Pettey, N. Currier, and H. Stark, Phys. Rev. E **57**, 610 (1998).

[30] B. I. Lev and P. M. Tomchuk, Phys. Rev. E **59**, 591 (1999).

[31] B. I. Lev, S. B. Chernyshuk, P. M. Tomchuk, and H. Yokoyama, Phys. Rev. E **65**, 021709 (2002).

[32] V. M. Pergamenshchik and V. O. Uzunova, Phys. Rev. E **76**, 011707 (2007).

[33] V. M. Pergamenshchik and V. A. Uzunova, Condens. Matter Phys. **13**, 33602 (2010).

[34] V. M. Pergamenshchik and V. A. Uzunova, Phys. Rev. E **83**, 021701 (2011).

[35] J. Fukuda, B. I. Lev, and H. Yokoyama, J. Phys.: Condens. Matter **15**, 3841 (2003).

[36] J. I. Fukuda and S. Žumer, Phys. Rev. E **79**, 041703 (2009).

[37] J. I. Fukuda, B. I. Lev, K. M. Aoki, and H. Yokoyama, Phys. Rev. E **66**, 051711 (2002).

[38] M. Oettel, A. Dominguez, M. Tasinkevych, and S. Dietrich, Eur. Phys. J. E **28**, 99 (2009).

[39] V. M. Pergamenshchik and V. A. Uzunova, Phys. Rev. E **79**, 021704 (2009).

[40] S. B. Chernyshuk and B. I. Lev, Phys. Rev. E **81**, 041701 (2010).

[41] S. B. Chernyshuk and B. I. Lev, Phys. Rev. E **84**, 011707 (2011).

[42] S. B. Chernyshuk, O. M. Tovkach, and B. I. Lev, Phys. Rev. E **85**, 011706 (2012).

[43] S. V. Shiyanovskii, A. Glushchenko, Yu. Reznikov, O. D. Lavrentovich, and J. L. West, Phys. Rev. E **62**, R1477 (2000).

[44] L. D. Landau and E. M. Lifshitz, *The Classical Theory of Fields*, 4th ed. (Butterworth-Heinemann, Oxford, 1994), p. 106.

[45] J. D. Jackson, *Classical Electrodynamics*, 3rd ed. (John Wiley & Sons, New York, 1998), p. 140.